

Statistically Efficient Bayesian Sequential Experiment Design via Reinforcement Learning with Cross-Entropy Estimators

Tom Blau^{1*} Iadine Chades² Amir Dezfouli^{3*} Daniel Steinberg⁴ Edwin V. Bonilla⁴

Abstract

Reinforcement learning can learn amortised design policies for designing sequences of experiments. However, current amortised methods rely on estimators of expected information gain (EIG) that require an exponential number of samples on the magnitude of the EIG to achieve an unbiased estimation. We propose the use of an alternative estimator based on the cross-entropy of the joint model distribution and a flexible proposal distribution. This proposal distribution approximates the true posterior of the model parameters given the experimental history and the design policy. Our method overcomes the exponential-sample complexity of previous approaches and provide more accurate estimates of high EIG values. More importantly, it allows learning of superior design policies, and is compatible with continuous and discrete design spaces, non-differentiable likelihoods and even implicit probabilistic models.

1. Introduction

A key challenge in science is to develop predictive models based on experimental observations. As far back as [Lindley \(1956\)](#) it has been recognised that experimental designs can be optimised to be maximally informative, under the assumptions of a Bayesian framework. Since then optimal experimental design has been applied to a wide variety of fields with different models and assumptions, including neuroscience ([Shababo et al., 2013](#)), biology ([Treloar et al., 2022](#)), ecology ([Drovandi et al., 2014](#)) and causal structure learning ([Agrawal et al., 2019](#)).

Under the framework of Bayesian optimal experimental design (BOED), we have a probabilistic model $p(y|\theta, d)$ where d is the design (e.g. where to measure), y is the

outcome (e.g. the measurement value) and θ are parameters over which we have a prior belief $p(\theta)$. The objective is to find the optimal design d^* that maximises the expected information gain (EIG), defined as:

$$\text{EIG}(d) := \mathbb{E}_{p(y|d)}[\text{H}(p(\theta)) - \text{H}(p(\theta|y, d))], \quad (1)$$

$$d^* = \arg \max_{d \in \mathcal{D}} \text{EIG}(d). \quad (2)$$

Where $\text{H}(\cdot)$ is the entropy of the given distribution. We see that naïve computation of the EIG requires an expectation over the marginal likelihood $p(y|d)$ and estimation of the posterior $p(\theta|y, d)$. Since sampling from $p(y|d)$ is typically intractable and there is usually no closed-form solution for the posterior, minimising this expression involves estimating a nested expectation numerically, which is challenging ([Rainforth et al., 2018](#)). Furthermore, we are often interested in conducting more than one experiment, in which case optimal designs must incorporate the outcomes of previous experiments sequentially ([Krause and Guestrin, 2007](#)).

In settings where computational or application-specific constraints demand fast deployment times, recent *amortised* methods have proved successful, as they learn an optimal design policy as a function of the experimental history instead of optimising each design in turn ([Blau et al., 2022](#); [Foster et al., 2021](#); [Ivanova et al., 2021](#)). Once trained, a policy can be reused to design experiments as many times as desired, thus amortising the cost of training. However, these methods have the drawback that they rely on maximising estimators of the EIG that require an exponential number of samples on the magnitude of the EIG to achieve an unbiased estimate ([McAllester and Stratos, 2020](#); [Poole et al., 2019](#)). Thus, their performance degrades in cases where the true EIG is large. To address this limitation, we propose a new amortised method, using reinforcement learning (RL) and a bound based on the cross-entropy of the joint model distribution and a flexible proposal distribution. This bound can be seen as the sequential version of the bounds proposed by [Barber and Agakov \(2004\)](#) and [Foster et al. \(2019\)](#). The proposal distribution approximates the true posterior of the model parameters given the experimental history and the design policy. Our method does not suffer from exponential sample complexity and is thus able to achieve higher

¹Nourish Ingredients, Sydney, Australia ²CSIRO's Environment, Brisbane, Australia ³BIMLOGIQ, Sydney, Australia ⁴CSIRO's Data61, Canberra & Sydney, Australia. * Work done while at CSIRO's Data61. Correspondence to: Edwin V. Bonilla <edwin.bonilla@csiro.au>.

EIG than prior art, especially in settings where the information gain of the optimal policy is large. Furthermore, unlike previous amortised methods, our method is generally applicable to continuous and discrete design spaces, non-differentiable likelihoods, and even implicit likelihoods. Our experiments show the benefits of our approach when compared to competitive baselines.

2. Amortised design of experiments

In Bayesian optimal experimental design (BOED) the goal is to identify the parameters of a probabilistic model by sending queries to that model. Let $p(y|\theta, d)$ be the model of concern, with some prior belief $p(\theta)$ regarding the value of parameters θ . As described above, an optimal design d^* is one that maximises the EIG as given by Equations (1) and (2), where computational intractabilities readily appear in the estimation of the marginal likelihood and the posterior distribution.

Furthermore, more challenging than optimising a single experiment is the problem of optimising an entire sequence of experiments $d_{1:T}$ where $T \in \mathbb{N}$ is some fixed budget. One promising approach for settings under strong computational constraints at deployment time is to optimise a design policy $\pi : \mathcal{H} \rightarrow \mathcal{D}$ that designs experiments conditioned on a history $h_t = (d_i, y_i)_{i=1}^t$. The computational cost of learning such a policy is high, but designing experiments with a trained policy is computationally efficient, requiring only a single forward pass of a neural network. Therefore the training cost is amortised over the lifetime of the policy, and this class of algorithms is known as *amortised* sequential design of experiments.

A recent amortised method proposed by Foster et al. (2021) optimises the so-called sequential prior contrastive estimator (sPCE):

$$\text{sPCE}(\pi, T) := \mathbb{E} \left[\log \frac{p(h_T|\theta_0, \pi)}{\frac{1}{L+1} \sum_{l=0}^L p(h_T|\theta_l, \pi)} \right], \quad (3)$$

where the expectation is taken over the joint $p(\theta_{0:L})p(h_T|\theta_0, \pi)$. It is easy to show that this estimator is a lower bound on the EIG. Moreover, we see that it requires an original sample $\theta_0 \sim p(\theta)$ and additional samples $\theta_{1:L}$ in the denominator to compute the nested expectations. These additional samples are crucial to the construction of the bounded estimator¹.

¹Foster et al. (2021) refer to these $\theta_{1:L}$ samples as *contrastive* as they can be seen as contrasts to the original sample θ_0 . Generally, contrastive samples are used in various problems in machine learning but notably in efficient learning of energy-based models (EBM). The basic idea is that one can learn EBMs by contrasting it with another distribution with known density (see, e.g., Gutmann and Hyvärinen, 2010).

Unfortunately, it has been shown that these types of bounds require a number of samples L that is exponential in the magnitude of the quantity being estimated (McAllester and Stratos, 2020). In other words, if the EIG of a policy is large, then computing an accurate contrastive bound is intractable. We emphasise here that the sample complexity of these estimators is exponential in the magnitude of the EIG, rather than in the number of dimensions. This is usually referred to as the “log-n curse” or “log-k curse” rather than “curse of dimensionality” (see, e.g. Chen et al., 2021a; Wang et al., 2022).

3. The sequential cross-entropy estimator

As described above, the limitation of requiring an exponentially large number of samples inherent to contrastive EIG estimators is exacerbated significantly in the *sequential* experimental design setting. To address this, we propose the use of a cross-entropy estimator. To recap, our joint model distribution over parameters θ and observation history h_T given a policy π guiding the selection of designs is

$$\begin{aligned} p(\theta, h_T|\pi) &= p(\theta) \prod_{t=1}^T p(d_t|\pi(y_{1:t-1}, d_{1:t-1}))p(y_t|\theta, d_t) \\ &= p(\theta) \prod_{t=1}^T p(h_t|\theta, \pi(h_{t-1})), \end{aligned} \quad (4)$$

where $d_t = \pi(h_{t-1})$ and $h_0 := \emptyset$. For the above model we have that the true EIG is given by (see Appendix A.1):

$$\text{EIG}(\pi, T) = \mathbb{E}_{p(\theta, h_T|\pi)} [\log p(\theta|h_T, \pi)] + H[p(\theta)], \quad (5)$$

which is, essentially, the sequential version of Equation (1) and, therefore, poses significant computational challenges. Our goal is then to obtain a tractable estimator of the EIG that avoids the exponentially large number of samples required by contrastive approaches. For this purpose, we introduce a proposal distribution $q(\theta|h_T, \pi)$ that approximates the true intractable posterior $p(\theta|h_T, \pi)$. Furthermore, we propose using the following estimator that relies on the cross-entropy of these two distributions, and we refer to it as the sequential cross-entropy estimator (sCEE):

$$\text{sCEE}(\pi, T) := \mathbb{E}_{p(\theta, h_T|\pi)} [\log q(\theta|h_T, \pi)] + H[p(\theta)]. \quad (6)$$

From Jensen’s inequality, it follows that the cross-entropy of two random variables is a lower bound for the self-entropy of either variable. By extending this to the sequential case, the following theorem shows that the sCEE is a lower bound of the true EIG:

Theorem 1 *Let $p(y|\theta, d)$ be a probabilistic model with prior $p(\theta)$. For an arbitrary fixed design policy π and sequence length T , the EIG of using π to design T experiments is denoted $\text{EIG}(\pi, T)$. Let $q(\theta|h_T, \pi)$ be a proposal*

distribution over parameters θ conditioned on experimental history h_T , and the sCEE bound as defined in Equation (6), we have that

$$\text{sCEE}(\pi, T) \leq \text{EIG}(\pi, T).$$

Proof A sketch of the proof follows here, with the full proof in Appendix A.1. The main idea is to rewrite the EIG as an expectation w.r.t. distribution $p(h_T, \theta|\pi)$, and then show that the difference between EIG and sCEE is an expectation over KL divergences. ■

An important result follows from the above theorem describing the nature of the lower bound.

Corollary 2 *The above bound is tight if and only if $q(\theta|h_T, \pi) = p(\theta|h_T, \pi)$. The bias of the sCEE estimator is $-\mathbb{E}_{h_T} [\text{KL} [p(\theta|h_T, \pi) \parallel q(\theta|h_T, \pi)]]$.*

This is straightforward to show (see Appendix A.2) and means that the quality of the estimation rests on how well the proposal distribution can match the true posterior, in terms of KL divergence. This compares remarkably favourably with the bias of other estimators such as sPCE, which has a bias of $|\text{EIG}| - \log L$, where L is the number of samples.

Relation to previous bounds: Our sCEE bound described above is the sequential version of the bound proposed by Barber and Agakov (2004), who used it for estimating mutual information in the context of information transmission over noisy channels. This bound is also referred to in Foster et al. (2019) as the variational posterior estimator, who used it for gradient-based experimental design in a non-sequential setting.

3.1. Proposal parameterization

To evaluate the sCEE, we sample from the joint $p(\theta, h_T|\pi)$ simply by rolling out the policy. Under mild assumptions, it can be shown that this Monte Carlo estimation approaches the true value of the sCEE at a rate of $O(\frac{1}{\sqrt{n}})$, where n is the number of samples (cf. Appendix A.3). We will parameterise the proposal distribution by a conditional normalising flow network (Winkler et al., 2019) with parameters κ and, therefore, refer to it using $q_\kappa(\cdot)$. Thus, we can maximise the sCEE w.r.t. κ using stochastic gradient descent. Note that we only need to optimise the negative cross-entropy term $\mathbb{E}_{p(\theta, h_T|\pi)} [\log q_\kappa(\theta|h_T, \pi)]$, since the prior entropy is constant. Details of the normalising flows used in our experiments are in Appendix F.

4. Experiment design with sCEE and reinforcement learning

Blau et al. (2022) have shown that the problem of learning an experiment design policy can be formulated as a spe-

cial case of a Markov decision process (MDP), which we will refer to as sequential experiment design MDP (SED-MDP). Thus, we implement our proposed sequential design of experiments method by using the sCEE bound in the formulation of the *reward function* within the reinforcement learning (RL) framework defined by Blau et al. (2022),

$$R(s_{t-1}, a_{t-1}, s_t, \theta) = \log q_\kappa(\theta|B_{\psi,t}, \pi_\phi) - \log q_\kappa(\theta|B_{\psi,t-1}, \pi_\phi), \quad (7)$$

where experimental designs correspond to policy actions $a_{t-1} = d_t$, and we have defined our proposal (approximate posterior) distribution as $q(\theta|h_t, \pi) := q_\kappa(\theta|B_{\psi,t}, \pi_\phi)$. Here $B_{\psi,t} = \sum_{i=1}^t \text{ENC}_\psi(y_i, d_i)$ maps history information to the system states, s_t , with a pooled summary from an encoder network $\text{ENC}_\psi(\cdot, \cdot)^2$.

Furthermore, the parameterisation of history given by $B_{\psi,t}$ yields a permutation invariant pooled representation that is fed into the policy *emitter* network³, $\pi_\phi(h_t) = \text{EMM}_\phi(B_{\psi,t})$. This permutation invariance induces a Markovian structure, making such a parameterisation efficient for use in an RL framework. See Appendix C for more details of the full formulation. Henceforth, we will refer to our method as RL-sCEE.

4.1. The RL-sCEE Algorithm

Policy and critic networks π_ϕ and \mathcal{C}_χ can be updated following the rules of the RL algorithm of our choice, using mini-batches of either off-policy or on-policy samples. In our experiments, we use the REDQ algorithm of Chen et al. (2021b). The posterior network $q_\kappa(\cdot)$ can be updated using the same mini-batches to maximise the log density of the observations under our posterior model. Note that this means rewards are now no longer fixed but depend on $q_\kappa(\cdot)$, and change with every update of the posterior parameters κ . The computational cost thus incurred can be minimised by lazy evaluation (Bloss et al., 1988): we only update each reward when we are about to use it to update the policy and critic networks of the RL agent. The procedure is summarised in Algorithm 1.

We propose to learn the parameterised design policy network π_ϕ and the proposal distribution $q_\kappa(\cdot)$ from data simultaneously. Since the reward function depends on $q_\kappa(\cdot)$, and the objective function of $q_\kappa(\cdot)$ in turn depends on π_ϕ , this leads to inherent instability, similar to the “deadly triad” that is often observed in value-based reinforcement learning (Van Hasselt et al., 2018). We therefore apply several stabilisation mechanisms to prevent the neural network esti-

²We note that this type of encoder was also used by Foster et al. (2021) and Blau et al. (2022).

³In practice we follow Blau et al. (2022) and learn a stochastic policy network that returns a distribution over designs, $\pi_\phi : \mathcal{H} \rightarrow \mathcal{P}_D(\mathcal{D})$.

Algorithm 1 RL-sCEE

Input: \mathcal{M} : SED-MDP, L_π : policy loss function, L_C : critic loss function. All as defined in Appendix C.
 Initialise replay buffer \mathcal{B}
while convergence criterion not reached **do**
 Generate rollouts $(s_{0:T}, a_{0:T}, \theta)^{1:N}$ using \mathcal{M} and π and push to \mathcal{B} .
 Sample mini-batch of size m from \mathcal{B}
 Compute posterior loss
 $L_q = -\frac{1}{m} \sum_{i=1}^m \log q_\kappa(\theta^i | B_{\psi,t}^i)$
 Take gradient step to minimise $\nabla_\kappa L_q$
 Compute rewards for mini-batch using Equation (7)
 Use mini-batch and rewards to compute L_π & L_C
 Take gradient step to minimise $\nabla_\phi L_\pi$ and $\nabla_\chi L_C$
end while

mators from diverging. Details of the stabilisation mechanisms and RL formulation are given in Appendix C.

4.2. Advantages of RL-sCEE

Our method based on the sCEE lower bound and RL delivers a number of advantages. **(i) Better sample complexity:** it does not require the use of contrastive samples, and hence does not suffer from the exponential sample complexity issue of the sPCE bound. Thus, sCEE can more closely estimate EIG when the true quantity is large, although estimation accuracy depends on learning a good posterior network $q_\kappa(\cdot)$. **(ii) Applicable to implicit models:** Furthermore, we see that the sCEE estimator, as defined in Equation (6), only requires sampling of the model distribution and avoids explicit log-likelihood computations $\log p(h_T | \theta, \pi)$. This means that our method is compatible with implicit likelihood models where the likelihood is a black-box or intractable and, therefore, can only be sampled but not evaluated explicitly. Interestingly, the sCEE bound is closely related to the sACE bound introduced in the appendices of Foster et al. (2021). We discuss this relationship in Appendix B. **(iii) Suitable for continuous and discrete design spaces:** Finally, similar to the method proposed in Blau et al. (2022), our approach using the sCEE estimator along with reinforcement learning, as described in Algorithm 1 (in Appendix C), can handle both continuous and discrete design spaces.

5. Experimental results

We evaluate our proposed method on (i) synthetic data; (ii) continuous designs and implicit likelihoods⁴ in behavioural economics under a constant elasticity of substitution (CES) problem and a (iii) source location problem; and (iv) dis-

⁴We simulate an implicit likelihood by withholding the explicit likelihood values $p(y|\theta, d)$ from the RL-sCEE and iDAD agents.

crete designs in a prey population problem. Description and details of these problems and their mathematical models are given in the subsequent subsections. We compare our method (RL-sCEE) to a number of baselines; RL with the sPCE bound (RL-sPCE; Blau et al., 2022), Deep Adaptive Design (DAD; Foster et al., 2021), implicit Deep Adaptive Design (iDAD; Ivanova et al., 2021), and a non-amortised sequential Monte Carlo experiment design approach (SMC-ED; Moffat et al., 2020). We also compare to two greedy baselines; one that maximises the variational PCE bound (VPCE; Foster et al., 2020), and one that samples designs uniformly at random (Random).

5.1. Accuracy of estimators on synthetic data

Given the theoretical results about sCEE and contrastive bounds, we expect that sCEE should perform well in situations where the EIG is large and $q_\kappa(\cdot)$ is easy to learn. To assess this, we evaluate the estimator on 7 experimental tasks which allow us to know the true EIG in closed form. The priors are isotropic Gaussians of the form $\mathcal{N}(\mu_0, \sigma_0 \mathbf{I}_k)$ and the likelihoods are similarly Gaussian with known isotropic covariance $\sigma \mathbf{I}_k$, where k is the number of dimensions. Each task has an experimental budget of $T = 10$ experiments. Thus we can manipulate k, σ_0 and σ to create tasks where the EIG of the optimal design is known exactly. See Appendix E.1 for details.

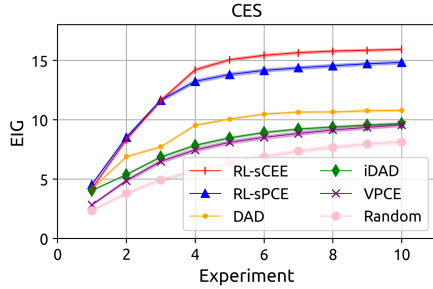
Table 1 enumerates these tasks, alongside the optimal EIG and the estimates of sCEE and sPCE with different numbers of contrastive samples. As can be seen from the left-most columns of the table, when the EIG is small enough, sPCE can provide a better estimate than sCEE (note that the sPCE at times slightly overestimates the EIG due to variance in estimating the expectation with Monte Carlo samples). However, as the EIG becomes large relative to $\log(L)$, the underestimation of sPCE becomes more severe, and for the right-most columns all sPCE variants have reached their upper limit. Meanwhile, sCEE consistently provides good estimates regardless of the magnitude of the EIG. It should be noted, however, that this is in part because in this experiment the posterior is easy to learn from data. We will evaluate more complex posteriors in the following sections.

5.2. Continuous designs

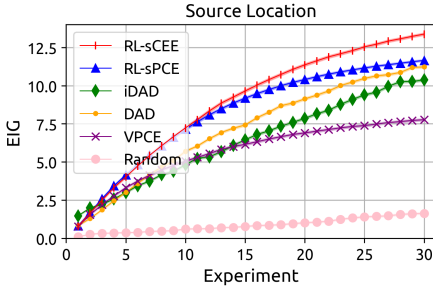
Constant elasticity of substitution (CES): Moving on to realistic tasks, we evaluate a design problem in behavioural economics where we must estimate the parameters of a Constant Elasticity of Substitution (CES) utility function (Baltas, 2001). Experimental designs consist of 2 bags of goods with 3 goods in each, so that the design space is $\mathcal{D} = [0, 100]^6$. The outcome is the relative preference of a test subject in the range $[0, 1]$, as determined by the agent’s CES utility function, and the specific values of its parameters $\theta = \{\rho, \alpha, u\}$,

Table 1. Different estimators for EIG of increasing magnitudes in synthetic data problems with conjugate priors. Averages computed over 1000 samples. k is the number of random variable dimensions, σ_0 is prior variance, and σ is likelihood variance.

Method	$k = 10$ $\sigma_0 = 0.5$ $\sigma = 5$	$k = 10$ $\sigma_0 = 0.5$ $\sigma = 1$	$k = 10$ $\sigma_0 = 1$ $\sigma = 1$	$k = 10$ $\sigma_0 = 2$ $\sigma = 1$	$k = 10$ $\sigma_0 = 2$ $\sigma = 0.5$	$k = 10$ $\sigma_0 = 4$ $\sigma = 0.5$	$k = 20$ $\sigma_0 = 4$ $\sigma = 0.5$
True EIG	3.47	8.96	11.99	15.22	18.57	21.97	43.94
sCEE	3.40	8.90	11.92	15.07	18.41	20.47	43.89
sPCE($L = 1\text{E}4$)	3.45	7.92	8.95	9.18	9.21	9.21	9.21
sPCE($L = 1\text{E}6$)	3.48	8.89	11.45	13.18	13.75	13.81	13.81
sPCE($L = 1\text{E}8$)	3.48	8.97	11.85	14.35	16.71	18.08	18.42



(a) CES experiment



(b) Source experiment

Figure 1. EIG for the CES and the source location problems, estimated using sPCE with $L = 1\text{E}8$. Trendlines are means and shaded regions are standard errors aggregated from 1000 rollouts. Our method is referred to as RL-sCEE.

with $\rho \in [0, 1]$, $\alpha \in \Delta_3$ and $u > 0$. See Appendix E.2 for full details.

Figure 1a shows the EIG achieved at each point in a sequence of $T = 10$ experiments. EIG was estimated by the sPCE estimator with $L = 1\text{E}8$ contrastive samples. Our proposed method, RL-sCEE, performs significantly better than all baselines. Indeed, by the 5th experiment, our method already exceeds the performance that the state-of-the-art RL-sPCE baseline attains after 10 experiments. Considering the sNMC upper bound shown in Table 2, it is clear that the *lower* bound for RL-sCEE is higher than the *upper* bound for RL-sPCE. This is particularly important since the EIG for the RL-sCEE policy is approaching the limits of what can be estimated by the lower bound, so that the gap between the true EIG and the estimate is potentially large.

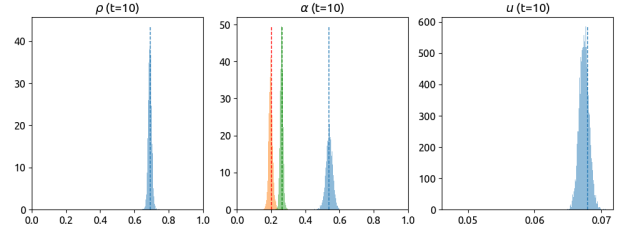


Figure 2. Example posterior distributions for the CES problem after 10 experiments. Histograms are based on $1\text{E}5$ samples. Dashed vertical lines indicate the ground truth value of each variable. The middle plot shows the marginals of the 3 different elements of α .

Since the conditional normalising flow q_κ is a posterior distribution, we can efficiently sample from it for any given history. It is important to note, however, that such posteriors can be expected to be accurate only for histories sampled from the joint $p(\theta, \pi_\phi)$ where π_ϕ is the stochastic policy network that was trained alongside $q_\kappa(\cdot)$. A representative posterior is shown in Figure 2. The histograms were computed using $1\text{E}5$ samples and 500 bins. The marginal distribution for each random variable is unimodal and highly concentrated. The mode of each marginal is very close to the true value of the corresponding random variable, denoted by a dashed vertical line of the same colour.

Posterior ablation: In order to test the efficacy of using the conditional normalising flow for the approximating the posteriors, $q_\kappa(\cdot)$, we compare it to using alternative parametrizations in Figure 3a. We use a Gaussian, and Gaussian mixture distributions with 2 and 3 components as alternatives. For the same wall-time (72 hours), the conditional normalising flow obtains a higher sCEE estimate of EIG even though fewer learning iterations are performed.

Source location: In the next experiment we consider the problem of locating signal sources in space. Here we have 2 sources with co-ordinates $s_1 = (x_1, y_1)$; $s_2 = (x_2, y_2)$, and designs consist of choosing the co-ordinates at which to take a noisy sample of signal magnitude. Signals decay with distance from the source and individual signals always superpose constructively. The full probabilistic model is described in Appendix E.4.

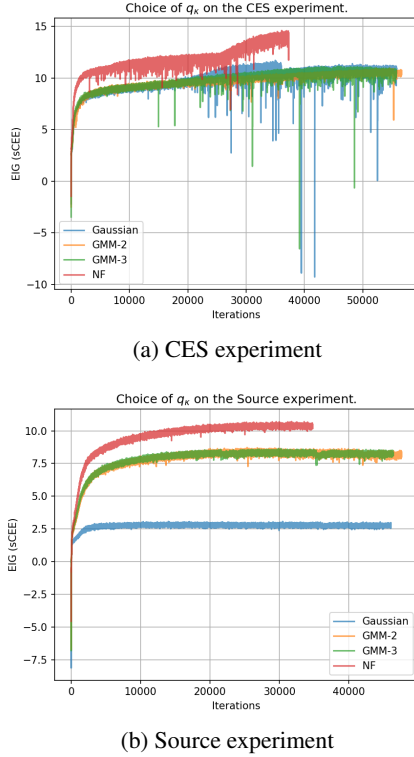


Figure 3. Influence of the choice of proposal distribution, $q_\kappa(\cdot)$, on the sCEE reward for a set wall-time limit. Figure 3a shows the CES experiment with $T = 10$ with a 72 hour wall-time limit. Figure 3b shows the Source experiment with $d = 2$ and $T = 30$ with a 60 hour wall-time limit. The proposal distributions are normalising flows (NF), Gaussian, and Gaussian mixtures with two and three components (GMM-2, GMM-3).

We trained policies to design sequences of $T = 30$ experiments. The mean and standard error of EIG achieved by our proposed method, as well as several baselines, are shown in Figure 1b. RL-sCEE outperforms all baselines by a statistically significant margin. As before, Table 2 shows that the lower bound estimate for our proposed method exceeds the upper bound estimate for all other methods.

As with the CES problem, we can examine the posterior obtained from $q_\kappa(\theta|h_T, \pi)$. This time, however, we plotted the marginals $q(x_1, x_2)$ and $q(y_1, y_2)$, i.e. the x and y coordinates of the 2 signal sources, using x_1 (respectively y_1) as the X-axis and x_2 (respectively y_2) as the Y-axis. The sources are exchangeable, i.e. $p(y|d, s_1 = (x_1, y_1), s_2 = (x_2, y_2)) = p(y|d, s_1 = (x_2, y_2), s_2 = (x_1, y_1))$. Therefore the marginals of the true Bayesian posterior, $p(x_1, x_2)$, should be symmetric w.r.t. the line $x_2 = x_1$ in the x_1x_2 -plane. Indeed, the plots in Figure 4 exhibit this symmetry, which has been learned entirely from data, without providing any inductive bias. We include a histogram of the full posterior in Appendix I.

Posterior ablation: Again, we test different characterisations

of the posterior, $q_\kappa(\cdot)$, to justify our choice of conditional normalising flows in Figure 3b. Our choice of conditional normalising flows performs better than all alternatives tested for estimating EIG with sCEE given a wall-time budget of 60 hours.

Dimensionality ablation: Here we compare how the sCEE and sPCE reward functions operate in higher dimensions in Table 3. This is a similar experiment as that conducted by Ivanova et al. (2021) (their Table 2), but we use an experimental sequence of $T = 30$. All estimators were run for a 60-hour wall time. We used the estimated training EIG to track the best model, which for $d = \{6, 10\}$ often occurred before the maximum training budget for both RL methods.

We found that RL-sCEE required more iterations before it converged compared to RL-sPCE, however RL-sCEE has a smaller memory footprint and so can be parallelized more readily. In order to fit some of the experiments into GPU memory (16GB), we had to reduce several aspects of our experimental settings (detailed in the caption of Table 3), therefore the numbers here are not comparable with those in Table 2.

In lower dimensional settings, where EIG is higher, the sCEE method outperforms sPCE. As we increase dimensionality sPCE outperforms sCEE perform similarly. This may be because sPCE is better at estimating lower EIGs as we saw in the synthetic data experiment.

Implicit likelihood: in both the CES and source location problem, we simulate an implicit likelihood by withholding the explicit likelihood values $p(y|\theta, d)$ from the RL-sCEE and iDAD agents. One would expect that both agents would perform worse than the RL-sPCE and DAD agents, which do exploit explicit likelihood information. Indeed, the iDAD agent is the least performant of any method considered. However, our proposed RL-sCEE method outperforms all baselines, both in the source location and CES problems, in spite of not having access to explicit likelihoods.

5.3. Discrete designs

To evaluate our method in tasks with discrete design spaces, we consider the prey population problem from Moffat et al. (2020). Designs are the initial population of a prey species, limited to the discrete interval $\mathcal{D} = 1, 2, \dots, 300$. The outcome is the number of individual who were consumed by predators at the end of a 24 hour period, based on the attack rate and handling time of the predators. Full details are available in Appendix E.3.

Since DAD and iDAD cannot optimise over discrete design spaces, we added the sequential Monte Carlo design algorithm proposed by Moffat et al. (2020) as a baseline. Note that this method is not amortised, and requires considerable computation time to design each experiment (> 1 minute

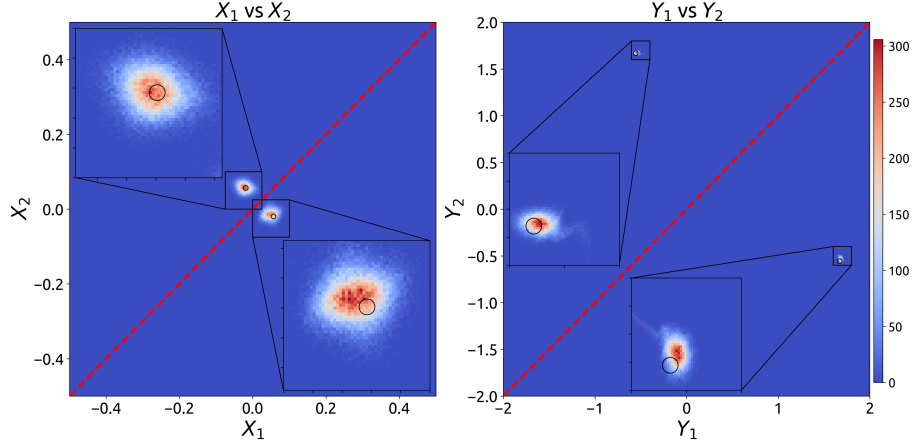


Figure 4. Histograms of example posteriors for the source location problem after 30 experiments, showing the joint distributions of the x co-ordinates (left) and y co-ordinates (right) of the 2 sources. The plots show symmetry with respect to the dashed red line, which is predicted by Bayes’ theorem. Insets zoom in on the modes of each posterior. Histograms are based on $1\text{E}5$ samples. Black rings denote the ground truth value of each variable.

Table 2. Lower and upper bounds for the EIG computed using the sPCE and sNMC estimators, respectively. $L = 1\text{E}8$ contrastive samples were used for the CES and Source Location problems, and $L = 1\text{E}6$ for the Prey Population problem. Means and standard errors aggregated from 1000 rollouts.

Method	CES		Source Location		Prey Population	
	Lower bound	Upper bound	Lower bound	Upper bound	Lower bound	Upper bound
RL-sCEE	15.91 \pm 0.10	20.78 \pm 0.43	13.37 \pm 0.07	13.42 \pm 0.08	4.41 \pm 0.05	4.41 \pm 0.05
RL-sPCE	14.81 \pm 0.12	15.56 \pm 0.17	11.65 \pm 0.06	12.01 \pm 0.07	4.38 \pm 0.05	4.41 \pm 0.04
DAD	10.77 \pm 0.08	13.20 \pm 0.68	11.22 \pm 0.07	11.29 \pm 0.07	N/A	N/A
iDAD	9.67 \pm 0.08	10.63 \pm 0.52	10.37 \pm 0.07	10.41 \pm 0.08	N/A	N/A
SMC-ED	N/A	N/A	N/A	N/A	4.52 \pm 0.07	4.52 \pm 0.06

Table 3. Behaviour of the estimators on the Source experiment with $T = 30$ in increasingly high dimensions. Lower and upper bounds for the EIG computed using the sPCE and sNMC estimators, respectively, with $L = 1\text{E}6$ contrastive samples and 1000 rollouts.

d	Method	EIG lower	EIG upper
2	RL-sCEE	12.31 \pm 0.06	14.29 \pm 0.16
	RL-sPCE	12.13 \pm 0.05	12.97 \pm 0.08
4	RL-sCEE	8.99 \pm 0.08	9.09 \pm 0.09
	RL-sPCE	8.87 \pm 0.08	8.98 \pm 0.09
6	RL-sCEE	4.37 \pm 0.08	4.37 \pm 0.08
	RL-sPCE	4.69 \pm 0.08	4.70 \pm 0.08
10	RL-sCEE	1.71 \pm 0.05	1.71 \pm 0.05
	RL-sPCE	1.85 \pm 0.05	1.85 \pm 0.05

per design, whereas amortised policies take milliseconds). As can be seen from Figure 5a, RL-sCEE performs similarly to the baselines, in spite of having no access to explicit likelihood information (a circumstance which would cause both baselines to fail) and using orders of magnitude less time to compute designs than the SMC-ED baseline. The numerical estimates in Table 2 show a relative difference of $\sim 1\%$ in the mean EIG estimates, and the standard errors overlap.

Finally, Figure 5b shows the posterior distributions after 10 experiments, with their corresponding priors. Both marginals place the mode near the true value of the random variable. The handling time (right) is fitted very tightly, whereas the attack rate (left) has a poorer fit. Both variables have the same prior, but the posterior for handling time is so concentrated that the prior is barely visible at the bottom of the plot.

6. Related work

Considerable work has been done on BOED (Chaloner and Verdinelli, 1995; Ryan et al., 2016), and particularly on using machine learning to optimise experimental designs (Rainforth et al., 2023). Greedy algorithms have been developed based on variational bounds (Foster et al., 2019; 2020) or neural network estimates (Kleinegesse and Gutmann, 2020) of the EIG. In the active learning literature, the BALD (Houlsby et al., 2011) score is equivalent to EIG, and can be estimated using Monte Carlo dropout neural networks (Gal et al., 2017). Other works attempt a non-greedy approach, i.e. they can sacrifice information gain in the current experiment in exchange for higher information gain in future experiments. Such approaches include

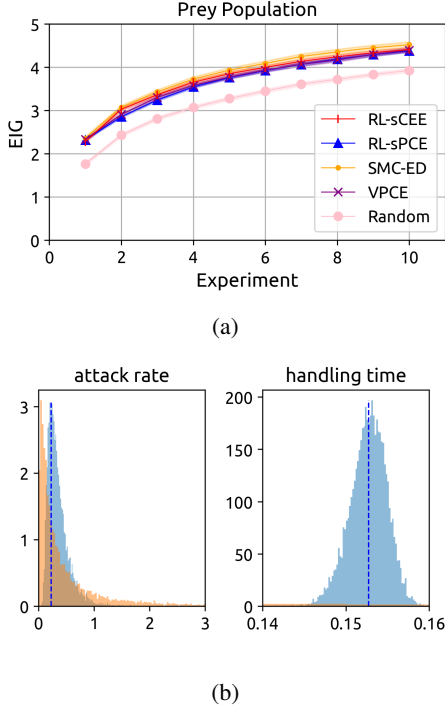


Figure 5. Figure 5a EIG for the prey population problem, estimated using sPCE with $L = 1\text{E}6$. Trendlines are means and shaded regions are standard errors aggregated from 1000 rollouts (RL) or 500 rollouts (SMC-ED). Figure 5b priors (orange) and posteriors (blue) after 10 experiments. Histograms used $1\text{E}5$ samples.

n-step look-ahead (Zhao et al., 2021; Yue and Kontar, 2020) or using batch designs as a lower bound for the utility of sequential designs (Jiang et al., 2020). Foster et al. (2021) were the first to propose an amortised method for sequential experiment design, and showed empirically that the learned policies can exhibit non-myopic behaviour. This was extended to the case of implicit likelihood models by Ivanova et al. (2021). Blau et al. (2022) formulated the sequential experimental design (SED) problem as a special MDP, and showed that design policies can be learned with RL algorithms.

There is also a similarity (up to the distribution of the expectation) between sCEE bound and the cross entropy objectives used in simulation-based inference (SBI) – in particular the amortized posterior variants (Cranmer et al., 2020) that admit implicit treatments of the likelihood function in the style of approximate Bayesian computation (ABC). Furthermore, cross entropy methods have a rich history in optimisation and importance sampling for rare event estimation and conditioning (Botev et al., 2013; Rubinstein, 1999; Miller et al., 2021; Brookes et al., 2019).

The field of Reinforcement Learning has two specialised frameworks for dealing with unknown parameters that govern the system dynamics: Bayes Adaptive MDPs (Duff,

2002) and Partially Observable MDPs (Kaelbling et al., 1998). In both cases, agents must balance between improving their posterior belief about the MDP and achieving high rewards. The variBAD (Zintgraf et al., 2021) algorithm fits a variational autoencoder to observed transitions and rewards, and its latent variables are used as input for the policy. The FORBES (Chen et al., 2022) algorithm, on the other hand, uses normalising flows to model beliefs over latent variables, transitions and rewards. MAX (Shyam et al., 2019) uses an ensemble model to generate synthetic data and compute information gain, which guides each policy action.

Finally, as mentioned in Section 3, our sCEE estimator is the sequential version of the bound proposed in (Barber and Agakov, 2004) and the variational posterior estimator of (Foster et al., 2019). Our work then focuses on its extension and usage in the sequential setting with RL and demonstrates its practical advantages with respect to previous amortised DOE methods, including that of (Blau et al., 2022).

7. Conclusions & limitations

We have introduced the sequential Cross-Entropy Estimator (sCEE), a lower bound estimate for the EIG of an experiment design policy, as well as a reinforcement learning algorithm (RL-sCEE) that uses it to optimise policies. We have shown that RL-sCEE can outperform or be comparable to state-of-the-art baselines.

RL-sCEE relies on learning a parameterized proposal network, $q_{\kappa}(\cdot)$, that closely matches the true posterior. In problems where this is challenging, the estimator bias could be large, and the design policies will be degraded. Furthermore, it is possible for a contrastive estimator to outdo sCEE with an extremely large number of samples. However, the cost of doing so during training, where millions of estimations are needed, is prohibitive for current hardware. Similarly, it is difficult to use the sCEE post-hoc for a policy that was not co-trained with the estimator, as this requires learning the policy network from scratch. Future work can focus on improving the learning of this proposal network.

Despite these limitations, we have shown that our method is highly flexible; it works with discrete design spaces, non-differentiable and implicit likelihood models. Surprisingly, our method even outperforms baselines that rely on explicit likelihoods.

Finally, our experiments show that the neural posterior proposal, $q_{\kappa}(\cdot)$, can learn significant structure that we know theoretically should be present in the true Bayesian posterior, such as symmetries or constraints on the support. This structure is learned entirely from data and self-guided experiments, with no inductive bias of any kind. And when the neural posterior proposal class may perform sub-optimally or additional information about the structure of the posterior

over θ is known, $q_{\kappa}(\cdot)$ can be trivially swapped out for more efficiently parameterized proposal distributions.

8. Impact Statement

This paper presents work whose goal is to advance the field of Machine Learning. There are many potential societal consequences of our work, none which we feel must be specifically highlighted here.

REFERENCES

- Agrawal, R., Squires, C., Yang, K., Shanmugam, K., and Uhler, C. (2019). Abcd-strategy: Budgeted experimental design for targeted causal structure discovery. In *International Conference on Artificial Intelligence and Statistics*.
- Baltas, G. (2001). Utility-consistent brand demand systems with endogenous category consumption: principles and marketing applications. *Decision Sciences*, 32(3):399–422.
- Barber, D. and Agakov, F. (2004). The IM algorithm: a variational approach to information maximization. In *Advances in neural information processing systems*.
- Bingham, E., Chen, J. P., Jankowiak, M., Obermeyer, F., Pradhan, N., Karaletsos, T., Singh, R., Szerlip, P., Horsfall, P., and Goodman, N. D. (2018). Pyro: Deep Universal Probabilistic Programming. *Journal of Machine Learning Research*.
- Blau, T., Bonilla, E. V., Chades, I., and Dezfouli, A. (2022). Optimizing sequential experimental design with deep reinforcement learning. In *International Conference on Machine Learning*.
- Bloss, A., Hudak, P., and Young, J. (1988). Code optimizations for lazy evaluation. *Lisp and Symbolic Computation*, 1(2):147–164.
- Botev, Z. I., Kroese, D. P., Rubinstein, R. Y., and L’Ecuyer, P. (2013). The cross-entropy method for optimization. In *Handbook of statistics*, volume 31, pages 35–59. Elsevier.
- Brookes, D., Park, H., and Listgarten, J. (2019). Conditioning by adaptive sampling for robust design. In *International conference on machine learning*, pages 773–782. PMLR.
- Chaloner, K. and Verdinelli, I. (1995). Bayesian experimental design: A review. *Statistical Science*, pages 273–304.
- Chen, J., Gan, Z., Li, X., Guo, Q., Chen, L., Gao, S., Chung, T., Xu, Y., Zeng, B., Lu, W., Li, F., Carin, L., and Tao, C. (2021a). Simpler, Faster, Stronger: Breaking The log-K Curse On Contrastive Learners With FlatNCE. pages 1–21.
- Chen, X., Mu, Y. M., Luo, P., Li, S., and Chen, J. (2022). Flow-based recurrent belief state learning for pomdps. In *International Conference on Machine Learning*, pages 3444–3468. PMLR.
- Chen, X., Wang, C., Zhou, Z., and Ross, K. W. (2021b). Randomized ensembled double q-learning: Learning fast without a model. In *International Conference on Learning Representations*.
- Cranmer, K., Brehmer, J., and Louppe, G. (2020). The frontier of simulation-based inference. *Proceedings of the National Academy of Sciences*, 117(48):30055–30062.
- Dinh, L., Sohl-Dickstein, J., and Bengio, S. (2017). Density estimation using real nvp. In *International Conference on Learning Representations*.
- Doshi-Velez, F. and Konidaris, G. (2016). Hidden parameter markov decision processes: A semiparametric regression approach for discovering latent task parametrizations. In *International Joint Conference on Artificial Intelligence*.
- Drovandi, C. C., McGree, J. M., and Pettitt, A. N. (2014). A sequential monte carlo algorithm to incorporate model uncertainty in Bayesian sequential design. *Journal of Computational and Graphical Statistics*, 23(1):3–24.
- Duff, M. O. (2002). *Optimal Learning: Computational procedures for Bayes-adaptive Markov decision processes*. University of Massachusetts Amherst.
- Foster, A., Ivanova, D. R., Malik, I., and Rainforth, T. (2021). Deep adaptive design: Amortizing sequential Bayesian experimental design. *International Conference on Machine Learning*.
- Foster, A., Jankowiak, M., Bingham, E., Horsfall, P., Teh, Y. W., Rainforth, T., and Goodman, N. (2019). Variational Bayesian optimal experimental design. In *Advances in Neural Information Processing Systems*.
- Foster, A., Jankowiak, M., O’Meara, M., Teh, Y. W., and Rainforth, T. (2020). A unified stochastic gradient approach to designing Bayesian-optimal experiments. In *International Conference on Artificial Intelligence and Statistics*.
- Gal, Y., Islam, R., and Ghahramani, Z. (2017). Deep Bayesian active learning with image data. In *International Conference on Machine Learning*.
- Garage Contributors (2019). Garage: A toolkit for reproducible reinforcement learning research. <https://github.com/rlworkgroup/garage>.
- Gutmann, M. and Hyvärinen, A. (2010). Noise-contrastive estimation: A new estimation principle for unnormalized

- statistical models. In Teh, Y. W. and Titterton, M., editors, *Proceedings of the Thirteenth International Conference on Artificial Intelligence and Statistics*, volume 9 of *Proceedings of Machine Learning Research*, pages 297–304, Chia Laguna Resort, Sardinia, Italy. PMLR.
- Houlsby, N., Huszár, F., Ghahramani, Z., and Lengyel, M. (2011). Bayesian active learning for classification and preference learning. *arXiv preprint arXiv:1112.5745*.
- Ivanova, D., Foster, A., Kleinegesse, S., Gutmann, M. U., and Rainforth, T. (2021). Implicit deep adaptive design: Policy-based experimental design without likelihoods. In *Advances in Neural Information Processing Systems*.
- Jiang, S., Chai, H., Gonzalez, J., and Garnett, R. (2020). Binoculars for efficient, nonmyopic sequential experimental design. In *International Conference on Machine Learning*.
- Kaelbling, L. P., Littman, M. L., and Cassandra, A. R. (1998). Planning and acting in partially observable stochastic domains. *Artificial intelligence*, 101(1-2):99–134.
- Kleinegesse, S. and Gutmann, M. U. (2020). Bayesian experimental design for implicit models by mutual information neural estimation. In *International Conference on Machine Learning*.
- Krause, A. and Guestrin, C. (2007). Nonmyopic active learning of gaussian processes: an exploration-exploitation approach. In *International Conference on Machine Learning*.
- Lillicrap, T. P., Hunt, J. J., Pritzel, A., Heess, N., Erez, T., Tassa, Y., Silver, D., and Wierstra, D. (2016). Continuous control with deep reinforcement learning. *International Conference on Learning Representations*.
- Lindley, D. V. (1956). On a measure of the information provided by an experiment. *The Annals of Mathematical Statistics*, pages 986–1005.
- McAllester, D. and Stratos, K. (2020). Formal limitations on the measurement of mutual information. In *International Conference on Artificial Intelligence and Statistics*.
- Miller, C., Corcoran, J. N., and Schneider, M. D. (2021). Rare events via cross-entropy population monte carlo. *IEEE Signal Processing Letters*, 29:439–443.
- Moffat, H., Hainy, M., Papanikolaou, N. E., and Drovandi, C. (2020). Sequential experimental design for predator-prey functional response experiments. *Journal of the Royal Society Interface*, 17(166).
- Poole, B., Ozair, S., Van Den Oord, A., Alemi, A., and Tucker, G. (2019). On variational bounds of mutual information. In *International Conference on Machine Learning*.
- Rainforth, T., Cornish, R., Yang, H., Warrington, A., and Wood, F. (2018). On nesting monte carlo estimators. In *International Conference on Machine Learning*.
- Rainforth, T., Foster, A., Ivanova, D. R., and Smith, F. B. (2023). Modern Bayesian experimental design. *arXiv preprint arXiv:2302.14545*.
- Rubinstein, R. (1999). The cross-entropy method for combinatorial and continuous optimization. *Methodology and computing in applied probability*, 1:127–190.
- Ryan, E. G., Drovandi, C. C., McGree, J. M., and Pettitt, A. N. (2016). A review of modern computational algorithms for Bayesian optimal design. *International Statistical Review*, 84(1):128–154.
- Shababo, B., Paige, B., Pakman, A., and Paninski, L. (2013). Bayesian inference and online experimental design for mapping neural microcircuits. *Advances in Neural Information Processing Systems*.
- Shyam, P., Jaśkowski, W., and Gomez, F. (2019). Model-based active exploration. In *International Conference on Machine Learning*.
- Stimper, V., Liu, D., Campbell, A., Berenz, V., Ryll, L., Schölkopf, B., and Hernández-Lobato, J. M. (2023). Normflows: A PyTorch Package for Normalizing Flows. *arXiv preprint arXiv:2302.12014*.
- Treloar, N. J., Braniff, N., Ingalls, B., and Barnes, C. P. (2022). Deep reinforcement learning for optimal experimental design in biology. *PLOS Computational Biology*, 18(11).
- Van Hasselt, H., Doron, Y., Strub, F., Hessel, M., Sonnerat, N., and Modayil, J. (2018). Deep reinforcement learning and the deadly triad. In *NeurIPS Deep Reinforcement Learning Workshop*.
- Wang, X., Al-Bashabsheh, A., Zhao, C., and Chan, C. (2022). Smoothed infonce: Breaking the log n curse without overshooting. In *2022 IEEE International Symposium on Information Theory (ISIT)*, pages 724–729.
- Winkler, C., Worrall, D., Hoogetboom, E., and Welling, M. (2019). Learning likelihoods with conditional normalizing flows. *arXiv preprint arXiv:1912.00042*.
- Yue, X. and Kontar, R. A. (2020). Why non-myopic Bayesian optimization is promising and how far should we look-ahead? a study via rollout. In *International Conference on Artificial Intelligence and Statistics*.

Zhao, G., Dougherty, E., Yoon, B.-J., Alexander, F., and Qian, X. (2021). Uncertainty-aware active learning for optimal Bayesian classifier. In *International Conference on Learning Representations*.

Zintgraf, L., Schulze, S., Lu, C., Feng, L., Igl, M., Shiarlis, K., Gal, Y., Hofmann, K., and Whiteson, S. (2021). Varibad: variational bayes-adaptive deep rl via meta-learning. *The Journal of Machine Learning Research*, 22(1):13198–13236.

A. Proofs

This appendix enumerates the proofs for the theorems, corollaries and other claims made in the main paper.

A.1. Proof of Theorem 1

Here we prove the main theorem of the paper, which is restated for convenience

Theorem 1 *Let $p(y|\theta, d)$ be a probabilistic model with prior $p(\theta)$. For an arbitrary fixed design policy π and sequence length T , the EIG of using π to design T experiments is denoted $\text{EIG}(\pi, T)$. Let $q(\theta|h_T, \pi)$ be a proposal distribution over parameters θ conditioned on experimental history h_T , and the sCEE bound is*

$$\text{sCEE}(\pi, T) := \mathbb{E}_{p(\theta, h_T|\pi)} [\log q(\theta|h_T, \pi)] + H[p(\theta)] \quad (8)$$

we have that

$$\text{sCEE}(\pi, T) \leq \text{EIG}(\pi, T) \quad (9)$$

Proof From Theorem 1 of Foster et al. (2021) we have that the EIG is:

$$\text{EIG}(\pi, T) = \mathbb{E}_{p(h_T, \theta|\pi)} [\log p(h_T|\theta, \pi) - \log p(h_T|\pi)] \quad (10)$$

This can be rewritten into a more convenient form:

$$\text{EIG}(\pi, T) = \mathbb{E}_{p(h_T, \theta|\pi)} \left[\log \frac{p(h_T|\theta, \pi)}{p(h_T|\pi)} \right] = \mathbb{E}_{p(h_T, \theta|\pi)} \left[\log \frac{p(h_T, \theta|\pi)}{p(h_T|\pi)p(\theta)} \right] \quad (11)$$

$$= \mathbb{E}_{p(h_T, \theta|\pi)} \left[\log \frac{p(\theta|h_T, \pi)p(h_T|\pi)}{p(\theta)p(h_T|\pi)} \right] = \mathbb{E}_{p(h_T, \theta|\pi)} \left[\log \frac{p(\theta|h_T, \pi)}{p(\theta)} \right] \quad (12)$$

$$= \mathbb{E}_{p(h_T, \theta|\pi)} [\log p(\theta|h_T, \pi) - \log p(\theta)] \quad (13)$$

$$= \mathbb{E}_{p(h_T, \theta|\pi)} [\log p(\theta|h_T, \pi)] + H[p(\theta)]. \quad (14)$$

We proceed to show that sCEE lower bounds this form. Consider the KL divergence between 2 conditional distributions given a fixed value y :

$$\text{KL}[p(x|y) \parallel q(x|y)] = \mathbb{E}_{p(x|y)} \left[\log \frac{p(x|y)}{q(x|y)} \right] \quad (15)$$

If y is not fixed but random we then take an expectation:

$$\mathbb{E}_{p(y)} [\text{KL}[p(x|y) \parallel q(x|y)]] = \mathbb{E}_{p(x|y)p(y)} \left[\log \frac{p(x|y)}{q(x|y)} \right] \quad (16)$$

$$= \mathbb{E}_{p(x, y)} \left[\log \frac{p(x|y)}{q(x|y)} \right] \quad (17)$$

$$= \mathbb{E}_{p(x, y)} [\log p(x|y) - \log q(x|y)] \quad (18)$$

rearranging the sides gives

$$\mathbb{E}_{p(x, y)} [\log q(x|y)] = \mathbb{E}_{p(x, y)} [\log p(x|y)] - \mathbb{E}_{p(y)} [\text{KL}[p(x|y) \parallel q(x|y)]] \quad (19)$$

$$\leq \mathbb{E}_{p(x, y)} [\log p(x|y)] \quad (20)$$

where the last line exploits the fact that the KL divergence is always non-negative. Plugging in $x = \theta$; $y = (h_T; \pi)$ yields the lower bound:

$$\mathbb{E}_{p(\theta, h_T, \pi)} [\log q(\theta|h_T, \pi)] \leq \mathbb{E}_{p(\theta, h_T, \pi)} [\log p(\theta|h_T, \pi)] \quad (21)$$

For a known policy π this becomes:

$$\mathbb{E}_{p(\theta, h_T|\pi)} [\log q(\theta|h_T, \pi)] \leq \mathbb{E}_{p(\theta, h_T|\pi)} [\log p(\theta|h_T, \pi)] \quad (22)$$

Adding the prior entropy to both sides yields:

$$\mathbb{E}_{p(\theta, h_T | \pi)} [\log q(\theta | h_T, \pi)] + H[p(\theta)] \leq \mathbb{E}_{p(\theta, h_T | \pi)} [\log p(\theta | h_T, \pi)] + H[p(\theta)]. \quad (23)$$

Finally, plugging in Equations (8) and (14) completes the proof:

$$\text{sCEE}(\pi, T) \leq \text{EIG}(\pi, T) \quad (24)$$

■

A.2. Proof of corollaries

In the main paper we state a corollary of the above theorem:

Corollary 2 *The bound is tight if and only if $p(\theta | h_T, \pi) = q(\theta | h_T, \pi)$, and the bias of the sCEE estimator is $-\mathbb{E}_{h_T} [\text{KL} [p(\theta | h_T, \pi) \parallel q(\theta | h_T, \pi)]]$*

If we subtract the lower bound from the EIG we get the difference:

$$\mathbb{E}_{p(\theta, h_T | \pi)} [\log p(\theta | h_T, \pi)] - \mathbb{E}_{p(\theta, h_T | \pi)} [\log q(\theta | h_T, \pi)]. \quad (25)$$

From Equation (19) it follows that this difference is

$$-\mathbb{E}_{h_T} [\text{KL} [p(\theta | h_T, \pi) \parallel q(\theta | h_T, \pi)]] \quad (26)$$

Since the KL divergence is always non-negative, this difference is 0 and the bound is tight if and only if $\text{KL} [p(\theta | h_T, \pi) \parallel q(\theta | h_T, \pi)] = 0$ for all realisations of h_T . This establishes both corollaries.

A.3. Proof of convergence

In the main paper we make the claim that a Monte Carlo estimator of the sCEE converges at a rate of $O(\frac{1}{\sqrt{n}})$, where n is the number of MC samples. Since the prior is known, we can rely on standard MC convergence proofs for the prior entropy component. Thus we need only worry about a convergence proof for estimating the cross-entropy component $\mathbb{E}_{p(\theta, h_T | \pi)} [\log q(\theta | h_T, \pi)]$. We denote the cross-entropy as $H[p(\theta | h_T, \pi), q(\theta | h_T, \pi)]$ and the MC estimator as

$$\hat{H}[p(\theta | h_T, \pi), q(\theta | h_T, \pi)] = \frac{1}{n} \sum_{i=1}^n -\log q(\theta^i | h_T^i, \pi) \quad (27)$$

According to Theorem 5.1 of [McAllester and Stratos \(2020\)](#), if there is a minimum log-likelihood F_{max} such that $\log q(\theta | h_T, \pi) \geq F_{max}$, then with probability at least $1 - \delta$ we have that

$$\left| H[p(\theta | h_T, \pi), q(\theta | h_T, \pi)] - \hat{H}[p(\theta | h_T, \pi), q(\theta | h_T, \pi)] \right| \leq F_{max} \sqrt{\frac{\log(\frac{2}{\delta})}{2n}} \quad (28)$$

Thus the MC estimator converges to the true sCEE with high probability at the desired rate of $O(\frac{1}{\sqrt{n}})$.

B. Relationship between sCEE and sACE

[Foster et al. \(2021\)](#) propose in the appendices a lower bound EIG estimator that relies on a parameterised proposal distribution that approximates the posterior $p(\theta | h_T)$. They called this the *sequential Adaptive Contrastive Estimation* (sACE):

$$\mathbb{E}_{p(\theta_0, h_T | \pi) q(\theta_{1:L}; h_T)} \left[\log \frac{p(h_T | \theta_0, \pi)}{\frac{1}{L+1} \sum_{l=0}^L \frac{p(h_T | \theta_l, \pi) p(\theta_l)}{q(\theta_l; h_T)}} \right] \quad (29)$$

This is a contrastive bound where the contrastive samples are distributed according to the proposal distribution $\theta_{1:L} \sim q(\theta|h_T)$. The construction and proof assume a minimum of 1 contrastive sample. However, if we set $L = 0$ in this expression, the sampling of contrastive samples from $q(\theta|h_T)$ disappears and we get:

$$\mathbb{E}_{p(\theta_0, h_T|\pi)} \left[\log \frac{p(h_T|\theta_0, \pi)}{\frac{1}{0+1} \sum_{l=0}^0 \frac{p(h_T|\theta_l, \pi)p(\theta_l)}{q(\theta_l; h_T)}} \right] = \mathbb{E}_{p(\theta_0, h_T|\pi)} \left[\log \frac{p(h_T|\theta_0, \pi)}{\frac{1}{0+1} \frac{p(h_T|\theta_0, \pi)p(\theta_0)}{q(\theta_0; h_T)}} \right] \quad (30)$$

$$= \mathbb{E}_{p(\theta_0, h_T|\pi)} \left[\log \frac{p(h_T|\theta_0, \pi) q(\theta_0; h_T)}{p(h_T|\theta_0, \pi) p(\theta_0)} \right] \quad (31)$$

$$= \mathbb{E}_{p(\theta_0, h_T|\pi)} \left[\log \frac{q(\theta_0; h_T)}{p(\theta_0)} \right], \quad (32)$$

which is equivalent to the sCEE. Note that by avoiding the need for contrastive samples, the sCEE gains a considerable computational advantage. In the RL setting, the rewards depend on $q(\theta|h_T)$ and hence need to be recomputed every time q is updated. With the sACE estimator, this recomputation requires resampling the contrastive samples, increasing the computational effort by a factor of $O(L)$. Indeed, depending on memory constraints, it may not be possible to recompute an entire batch of rewards in a single vectorised operation. With the sCEE, however, reward recomputation requires only a single neural network pass.

In addition to the computational benefits, sCEE has the further advantage that it is compatible with implicit likelihood models, whereas sACE requires explicit models, since it includes the term $p(h_T|\theta_0, \pi)$ in the numerator.

C. Reinforcement learning algorithm

Blau et al. (2022) have shown that the problem of learning an experiment design policy can be formulated as a special case of a MDP called the SED-MDP. We follow their formulation for the reinforcement learning algorithm in this paper, with the main difference being the use of the sCEE reward and consequently the use of an approximate proposal $q_\kappa(\theta|h_T)$ parameterised as a conditional normalising flows neural network (Winkler et al., 2019) with parameters κ .

The SED-MDP is a hidden parameter MDP (Doshi-Velez and Konidaris, 2016) which is a tuple of the form $\mathcal{M} = (\mathcal{S}, \mathcal{A}, \Theta, \text{Tr}, \text{R}, \gamma, P_\Theta)$ where,

- \mathcal{S} , the system state, corresponds to the space of histories, \mathcal{H} ,
- \mathcal{A} , the action space, and corresponds to the design space, \mathcal{D} ,
- Θ is the space of unobserved parameters, θ ,
- $\text{Tr} : \mathcal{S} \times \mathcal{A} \rightarrow \mathcal{P}_\mathcal{S}(\mathcal{S})$ are the transition dynamics, and correspond to the pooled history encoder, $B_{\psi, t}$,
- $\text{R} : \mathcal{S} \times \mathcal{A} \times \mathcal{S} \rightarrow \mathbb{R}$: is reward function, and corresponds to Equation (7),
- $\gamma \in (0, 1]$ is a discount factor applied to rewards,
- P_θ is a prior over the parameter space, and is chosen to be $p(\theta)$ at the beginning of the episode.

The aim is to then find a policy, $\pi^* : \mathcal{S} \rightarrow \mathcal{P}_\mathcal{A}(\mathcal{A})$, that maximizes the expected discounted return,

$$J(\pi) := \mathbb{E} \left[\sum_{t=1}^T \gamma^{t-1} \text{R}(s_{t-1}, a_{t-1}, s_t) \right], \quad (33)$$

over a time horizon, T , and the expectation is over all probabilistic quantities in the tuple.

The posterior network $q_\kappa(\cdot)$ can be updated by using the same mini-batches to maximise the log-likelihood of the observations under our posterior model. Note that this means rewards are now no longer fixed but depend on $q_\kappa(\cdot)$, and change with every update of κ . The computational cost thus incurred can be minimised by lazy evaluation (Bloss et al., 1988): we only update each reward when we are about to use it to update the policy and critic networks of the RL agent. The procedure is summarised in Algorithm 1, and we give more details about this procedure in the following sections.

C.1. Simultaneous policy and reward learning

We propose to learn the design policy network π_ϕ and the proposal distribution $q_\kappa(\cdot)$ from data simultaneously. Since the reward function depends on $q_\kappa(\cdot)$, and the objective function of $q_\kappa(\cdot)$ in turn depends on π_ϕ , this leads to inherent instability, similar to the “deadly triad” that is often observed in value-based reinforcement learning (Van Hasselt et al., 2018). We therefore apply several stabilisation mechanisms to prevent the neural network estimators from diverging.

Target posterior network: similar to the use of target Q-networks as introduced by Lillicrap et al. (2016), we maintain a primary posterior network q_κ and a target network q'_κ . The primary network q_κ is updated using gradient descent in every iteration of the algorithm, but is not used directly to compute rewards. Instead, the target network q'_κ is used to compute Equation (7), and its weights are periodically updated to maintain a moving average:

$$\kappa' \leftarrow \kappa' \cdot (1 - \tau) + \kappa \cdot \tau \quad (34)$$

where $\tau \in (0, 1)$ is a constant controlling the rate of change.

Fixed initial posterior: the reward definition of Equation (7) assigns each experiment its own (estimated) information gain. The return of an entire trajectory is a telescoping sum that reduces to $\log q(\theta|B_{\psi,T}, \pi_\phi) - \log q(\theta|B_{\psi,0})$, and the expected return over infinitely many trajectories recovers the sCEE. Therefore, the component $q(\theta|B_{\psi,0})$ of the first reward r_0 is the only contributor to the prior entropy term $H[p(\theta)]$ of the sCEE. Since this term is constant w.r.t. all networks, we can simply ignore it when training as it does not change the optimal policy. Furthermore, learning the correct estimator for $q(\theta|B_{\psi,0})$ that maps the null inputs to the prior $p(\theta)$ can be challenging. Therefore instead of learning this mapping for the empty first state, we assigned it a fixed value of $\log q(\theta|B_{\psi,0}) := 0$.

C.2. Implementation

We use the Randomized ensembled double q-learning (REDQ) soft actor critic method from (Chen et al., 2021b), specifically that given in Algorithm 1 in their paper. Accordingly the actor and critic losses, L_π and L_C respectively, are given on lines 10 and 12 in their Algorithm 1, using the reward we have defined in Equation (7).

D. Normalising flows on the probability simplex

If we have a random variable with support on the canonical (open) simplex Δ_{k-1} rather than in \mathcal{R}^k , additional caution is required for fitting a normalising flow to this RV. Since the k^{th} dimension of the RV is fully determined by the first $k - 1$ dimensions, the NF is free to fit this dimension with extremely high confidence, leading to an overestimation of log-likelihood of the entire RV.

The fix to this issue is rather involved. First, we exclude the k^{th} dimension as input to the NF. Then, at the penultimate layer of a normalising flow, it implements the diffeomorphism $\mathcal{F} : \mathcal{R}^{k-1} \rightarrow \mathcal{R}^{k-1}$ i.e. the base distribution is a standard Gaussian and the resulting distribution can have support in the entire real space. Now we add a series of bijections that will produce a map $\mathcal{G} : \mathcal{R}^{k-1} \rightarrow \Delta_{k-1}$. Note that it is not enough simply to concatenate $1 - \sum_{i=1}^{k-1} \mathcal{F}(x)_i$ with the intermediate vector $\mathcal{F}(x)$ because we are not guaranteed that $0 \leq \mathcal{F}(x)_k \leq 1 \forall k$ and that $\sum_{i=1}^{k-1} \mathcal{F}(x)_i \leq 1$. First we must transform the output to ensure these properties:

$$u = \mathcal{F}(x) \quad (35)$$

$$v_i = \sigma(u_i) \quad (36)$$

$$w_i = v_i \left(1 - \sum_{j=1}^{i-1} w_j \right) \quad \forall i \in [1, k-1] \quad (37)$$

$$\theta_i = \frac{w_i}{1 - \epsilon}. \quad (38)$$

Equation (36) projects \mathcal{R}^{k-1} to the semi-open box $[0, 1)^{k-1}$. Equation (37) projects this box to the $k - 1$ dimensional simplex $s = \{x : \sum_{i=1}^{k-1} x_i < 1 \text{ and } 0 \leq x_k < 1 \forall i \in [1, k-1]\}$. This non-canonical simplex is in fact the equivalent of projecting the k -dimensional canonical simplex Δ_{k-1} down to $k - 1$ dimensions. The simplex s can be lifted to Δ_{k-1} by

assigning $w_k = 1 - \sum_{j=1}^{k-1} w_j$. However, we won't include this in the mapping \mathcal{G} because it makes the Jacobian low-rank and hence the inverse ill-defined. To avoid floating-point errors, each element of the RV actually has to be in the range $[\epsilon, 1 - \epsilon]$ where ϵ is the machine epsilon. Equation (38) maps between this space and the actual canonical simplex.

The corresponding log-det-Jacobians are:

$$\sum_{i=1}^{k-1} \log(0.99 \cdot v_i(1 - v_i)), \quad (39)$$

$$\sum_{i=1}^{k-1} \log(1 - \sum_{j=1}^{i-1} w_j), \quad (40)$$

$$(1 - k) \cdot \log(1 - \epsilon). \quad (41)$$

The inverse \mathcal{G}^{-1} can be written compactly as:

$$u_i = \sigma^{-1} \left(\frac{(1 - \epsilon) \cdot \theta_i}{1 - \sum_{j=1}^{i-1} (1 - \epsilon) \cdot \theta_j} \right) \quad \forall i \in [1, k - 1]. \quad (42)$$

E. Experiment details

This appendix describes the probabilistic models, hyperparameters, and all other details relating to the experiment design problems appearing in the paper.

We implemented our algorithm using Pyro (Bingham et al., 2018) and normflows (Stimper et al., 2023) along with the Garage framework (Garage Contributors, 2019) and the REDQ algorithm (Chen et al., 2021b) for reinforcement learning. For complete details about algorithms and hyperparameters, see Appendix F.

E.1. Synthetic data – EIG for conjugate priors

For an isotropic Gaussian prior $\mathcal{N}(\mu_0, \sigma_0 \mathbf{I}_k)$ and Gaussian likelihood with known isotropic covariance $\sigma \mathbf{I}_k$, the posterior after n observations is an isotropic Gaussian with covariance:

$$\Sigma_{post} = (\sigma_0^{-1} \mathbf{I}_k + n\sigma^{-1} \mathbf{I}_k)^{-1} \quad (43)$$

$$= (\sigma_0^{-1} + n\sigma^{-1})^{-1} \mathbf{I}_k \quad (44)$$

The mean of the posterior is unimportant to us as it does not affect the entropy:

$$H_{post} = \frac{k}{2} + \frac{k}{2} \log(2\pi) + \frac{1}{2} \log(|\Sigma_{post}|) \quad (45)$$

$$= \frac{k}{2} + \frac{k}{2} \log(2\pi) - \frac{k}{2} \log(\sigma_0^{-1} + n\sigma^{-1}). \quad (46)$$

Therefore the entropy is independent of the designs and we can compute the entropy of the “optimal” policy by subtracting the posterior entropy from the prior entropy:

$$I_n(\pi) = H[\mathcal{N}(\mu_0, \sigma_0 \mathbf{I}_k)] - H_{post} \quad (47)$$

$$= \cancel{\frac{k}{2}} + \cancel{\frac{k}{2} \log(2\pi)} + \frac{k}{2} \log(\sigma_0) - \cancel{\frac{k}{2}} - \cancel{\frac{k}{2} \log(2\pi)} + \frac{k}{2} \log(\sigma_0^{-1} + n\sigma^{-1}) \quad (48)$$

$$= \frac{k}{2} (\log(\sigma_0) + \log(\sigma_0^{-1} + n\sigma^{-1})) \quad (49)$$

$$= \frac{k}{2} \log(1 + n \frac{\sigma_0}{\sigma}) \quad (50)$$

Thus we can create an EIG estimation problem with an EIG of our choice by setting k, n, σ_0 and σ appropriately. In our experiments sCEE was trained for 10,000 epochs, and was exposed to 10,000 data points in each epoch. Each estimator was evaluated using 1,000 Monte Carlo samples.

E.2. Constant elasticity of substitution

We evaluate a design problem in behavioural economics where we must estimate the parameters of a Constant Elasticity of Substitution (CES) utility function (Baltas, 2001). In this experiment economic agents compare 2 baskets of goods and give a rating on a sliding scale from 0 to 1. Each basket consists of k different goods with different value. We set $k = 3$.

The outcome is the relative preference of a test subject in the range $[0, 1]$, as determined by the agent's CES utility function, and the specific values of its parameters $\theta = \{\rho, \alpha, u\}$, with $\rho \in [0, 1]$, $\alpha \in \Delta_3$ and $u > 0$.

The designs are vectors $d = (x, x')$ where $x, x' \in [0, 100]^k$ are the baskets of goods. The latent parameters of the likelihood and their priors are:

$$\rho \sim \text{Beta}(1, 1) \quad (51)$$

$$\alpha \sim \text{Dirichlet}(\mathbf{1}_k) \quad (52)$$

$$\log u \sim \mathcal{N}(1, 3). \quad (53)$$

The probabilistic model is:

$$U(x) = \left(\sum_i x_i^\rho \alpha_i \right)^{1/\rho} \quad (54)$$

$$\mu_\eta = (U(x) - U(x'))u \quad (55)$$

$$\sigma_\eta = (1 + \|x - x'\|)\tau \cdot u \quad (56)$$

$$\eta \sim \mathcal{N}(\mu_\eta, \sigma_\eta^2) \quad (57)$$

$$y = \text{clip}(\text{sigmoid}(\eta), \epsilon, 1 - \epsilon), \quad (58)$$

In our experiments we used the following hyperparameters:

PARAMETER	VALUE
k	3
τ	0.005
ϵ	2^{-22}

E.3. Prey population

In this experiment an initial population of prey animals is left to survive for \mathcal{T} hours, and we measure the number of individuals consumed by predators at the end of the experiment. The designs are the initial populations $d = N_0 \in 1, 2, \dots, 300$. The latent parameters and priors are:

$$\log a \sim \mathcal{N}(-1.4, 1.35) \quad (59)$$

$$\log T_h \sim \mathcal{N}(-1.4, 1.35), \quad (60)$$

where a represents the attack rate and T_h is the handling time.

The population changes over time according to a Holling's Type III model, which is a differential equation:

$$\frac{dN}{d\tau} = -\frac{aN^2}{1 + aT_hN^2}. \quad (61)$$

And the population $N_{\mathcal{T}}$ is thus the solution of an initial value problem. The probabilistic model is:

$$p_{\mathcal{T}} = \frac{d - N_{\mathcal{T}}}{d} \quad (62)$$

$$y \sim \text{Binom}(d, p_{\mathcal{T}}). \quad (63)$$

We used a simulation time of $\mathcal{T} = 24$ hours.

E.4. Source location

In this experiment there are n sources embedded in k -dimensional space that emit independent signals. the designs are the co-ordinates at which to measure signal intensity, and we restrict the space to $d \in [-4, 4]^k$. The total intensity at any given co-ordinate d in the plane is given the sum of individual signals:

$$\mu(\theta, d) = b + \sum_i \frac{1}{m + \|\theta_i - d\|^2}, \quad (64)$$

where $b, m > 0$ are the background and maximum signals, respectively, $\|\cdot\|^2$ is the squared Euclidean norm, and θ_i are the co-ordinates of the i^{th} signal source. The probabilistic model is:

$$\theta_i \sim \mathcal{N}(0, I); \quad \log y | \theta, d \sim \mathcal{N}(\log(\mu(\theta, d)), \sigma), \quad (65)$$

i.e. the prior is unit Gaussian and we observe the log of the total signal intensity with some Gaussian observation noise σ . The hyperparameters we used are:

PARAMETER	VALUE
n	2
k	2
b	1E - 1
m	1E - 4
σ	0.5

F. Algorithm experimental details

This appendix provides the implementation details for all design of experiment algorithms used in the paper.

F.1. RL-sCEE

We used the implementation of REDQ from [Blau et al. \(2022\)](#) as the basis of our algorithm, although we limited the ensemble size to $N = 2$. Normalising flows were implemented using the normflows ([Stimper et al., 2023](#)) package, which we extended to create a conditioned version of realNVP ([Dinh et al., 2017](#)). In every experiment we used a normalising flow with 6 layers, and the parameter map is a 2-layer neural network with sizes (128, 128). Both normalising flows and policies use a permutation invariant representation similar to [Ivanova et al. \(2021\)](#), including a single self-attention layer with 8 attention heads.

Additional hyperparameters are listed in the table below, and are largely derived from [Blau et al. \(2022\)](#):

For the Source Location experiments where $d = \{6, 10\}$, we had to reduce the buffer size from 1E7 to 1E6 in order to fit the estimators in the available 16GB of GPU memory.

F.2. RL-sPCE

We used the implementation of [Blau et al. \(2022\)](#), which is available at <https://github.com/csiro-mlai/rl-boed>. We kept all hyperparameters and network architectures the same, with the exception of adding a self-attention layer

PARAMETER	SOURCE LOCATION	CES	PREY POPULATION
TRAINING ITERATIONS	1E5	1E5	2E4
T	30	10	10
γ	0.9	0.9	0.95
τ	$1E - 3$	$5E - 3$	$1E - 2$
POLICY LEARNING RATE	$1E - 4$	$3E - 4$	$1E - 4$
CRITIC LEARNING RATE	$3E - 4$	$3E - 4$	$1E - 3$
BUFFER SIZE	1E7	1E7	1E6

to the policy network. This layer is identical to the one described in the previous section. We did not find that adding attention lead to significant change in performance, but included it in order to maintain a fair comparison with the RL-sCEE implementation.

In particular, we used $L = 1E5$ contrastive samples for training. Not only is it the value used by [Blau et al. \(2022\)](#), but is also pushing the limits of the number of samples that can be used in a reasonable amount of time. Since tens of millions of simulated experiments have to be run to train a single agent, we must leverage vectorisation over multiple sequences of experiments in parallel. Although in the evaluation we used $L = 1E8$ samples, this only allows a single experiment at a time to fit in a GPU, and requires multiple seconds per experiment. It would require several years to train a single agent in this manner.

F.3. DAD and iDAD

For these baselines we used the implementations of the original papers, which are available at <https://github.com/ae-foster/dad> and <https://github.com/desi-ivanova/idad>, respectively. We kept the default hyperparameters of those implementations. The only exception is for iDAD on the source location problem, which we found unstable for a sequence of $T = 30$ experiments. We therefore used early stopping, and stopped learning at $40k$ iterations instead of the original $100k$.

F.4. SMC-ED

We used the implementation made available in <https://github.com/csiro-mlai/rl-boed>, which in turn uses the R language implementation of ([Moffat et al., 2020](#)) and executes it from within a Python script by using the *rpy2* bindings. The original R code is available at https://github.com/haydenmoffat/sequential_design_for_predator_prey_experiments.

G. Hardware details

SMC-ED experiments were run on a desktop machine with an Intel i7-10610U CPU and no GPU. All other experiments were run in a high-performance computing cluster, using a single node each with 4 cores of an Intel Xeon E5-2690 CPU and an Nvidia Tesla P100 GPU with 16GB of VRAM.

H. Ablation study of stabilisation mechanisms

To evaluated the stabilisation mechanisms incorporated in the implementation of RL-sCEE, we conduct an ablation study where we remove either the target posterior network, the fixed initial posterior, or both. The results can be seen in Figure 6, with each variant replicated 10 times, using common random seeds between different variants (e.g. the blue trendline labeled "0" represents the same random seed in all 4 plots).

It is clear that the removal of the target network causes significant degradation in performance, with many replications converging to a lower final performance or even peaking early and then decreasing in EIG. On the other hand, the use of a fixed initial posterior doesn't seem to offer a clear advantage over a learned one.

I. Additional results

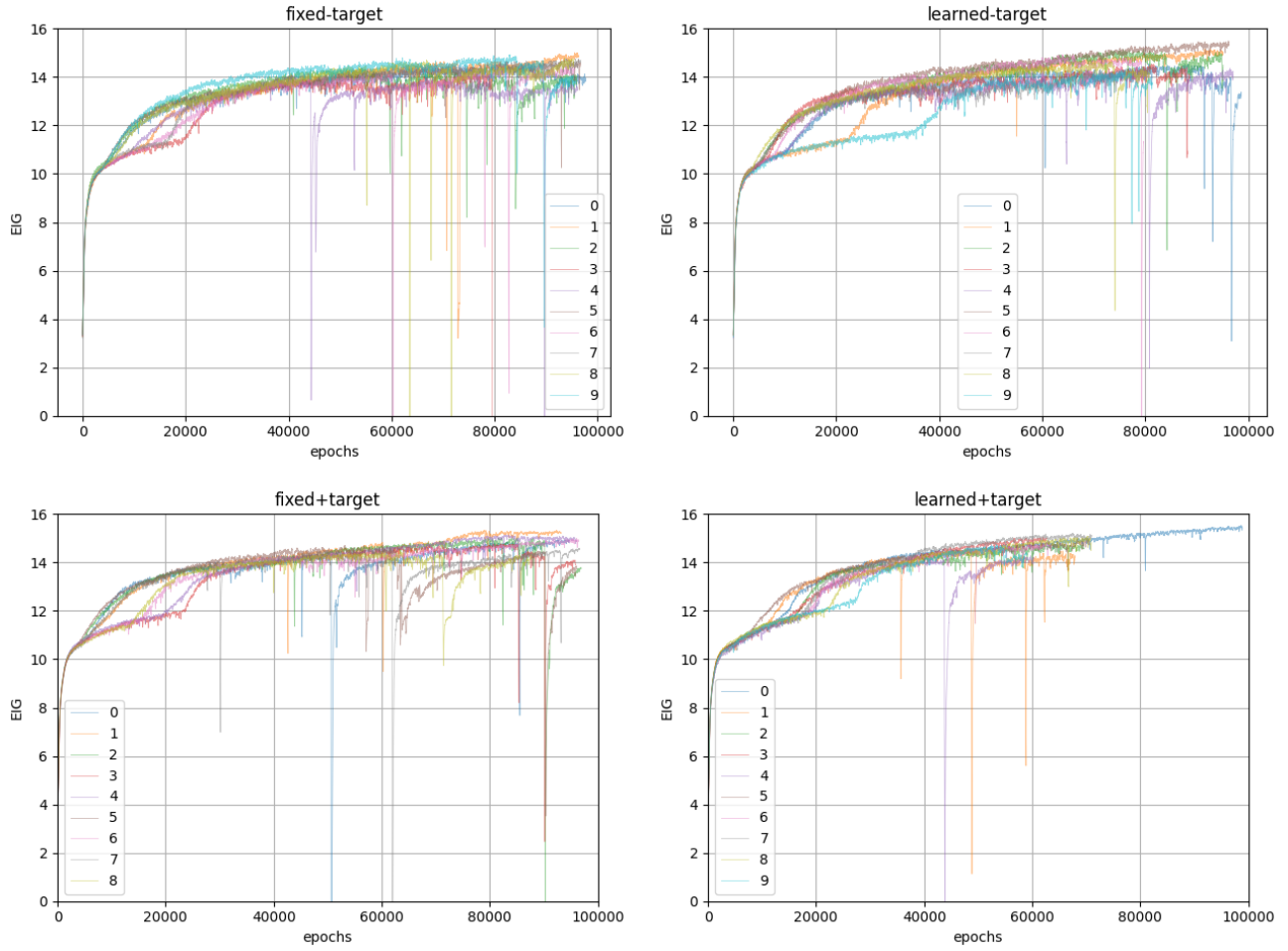


Figure 6. Ablation studies for the stabilisation mechanisms.

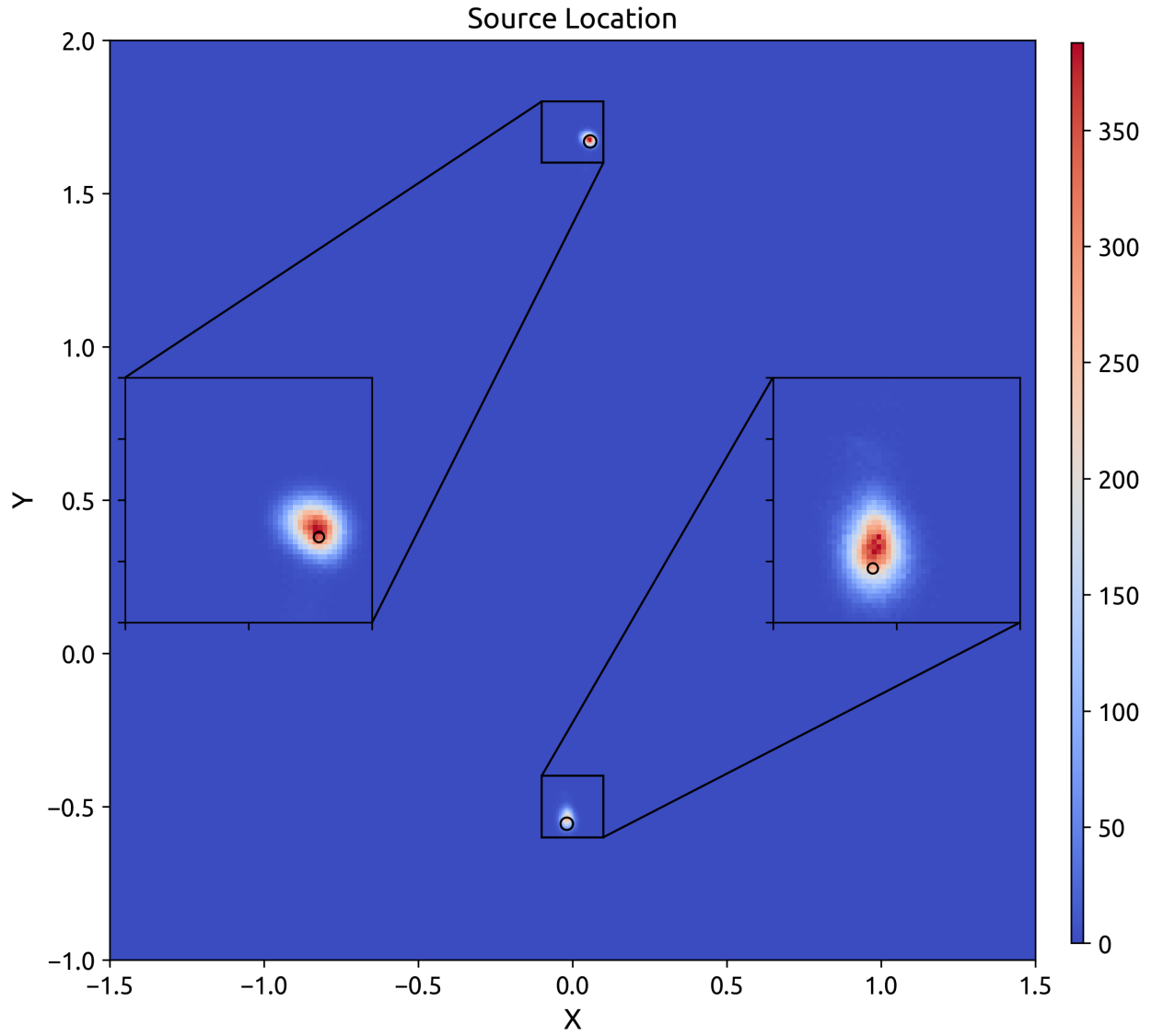


Figure 7. Posterior for the source location problem. Computed from $1E5$ samples. Black rings denote the true co-ordinates of signal sources.